Journal of Alloys and Compounds 509S (2011) S658–S661

Contents lists available at ScienceDirect

Journal of Alloys and Compounds

journal homepage: www.elsevier.com/locate/jallcom

Stability and mobility of native point defects in AlH_3

Lars Ismer*, Anderson Janotti, Chris G. Van de Walle

Materials Department, University of California, Santa Barbara, CA 93106-5050, USA

ARTICLE INFO

Article history:
Received 31 July 2010
Received in revised form 4 October 2010
Accepted 6 October 2010
Available online 15 October 2010

Keywords:
Hydrogen storage
Aluminum hydride
Point defects
Hybrid functional
Dehydrogenation
Activation energy
Band gap

ABSTRACT

We investigate the properties of native point defects in AlH_3 using density functional theory (DFT). The results indicate that mass transport in AlH_3 is mediated by positively charged hydrogen vacancies (V_H^+), with an activation energy of 1.72 eV that is in good agreement with experimentally observed values for the dehydrogenation of AlH_3. An accurate description of the point-defect properties requires use of an advanced hybrid DFT/Hartree–Fock approach with the functional of Heyd, Scuseria, and Enzerhof (HSE), as revealed by a detailed comparison with results obtained using a conventional generalized gradient approximation functional. The HSE produces a more accurate band gap, and significant differences are found for the formation energies of the defects between HSE and PBE. We discuss the differences in terms of an alignment of the band structures and defect transition levels on an absolute energy scale.

1. Introduction

Aluminum hydride (AlH_3) shows outstanding features as a hydrogen storage medium, with large volumetric and gravimetric hydrogen capacities. Furthermore, it has a low decomposition temperature, a low activation heat, and rapid dehydrogenation kinetics [1]. Unfortunately, its poor hydrogenation properties, which are due to the unfavorable thermodynamics of AlH_3 [2–6] and related to the low solubility of hydrogen in aluminum metal [7,8], have been a major obstacle to using AlH_3 in hydrogen-fueled cars. However, recently considerable progress has been made to overcome these obstacles [9]. Due to its outstanding dehydrogenation properties, AlH_3 is therefore considered a major candidate for hydrogen storage applications [1,9].

The dehydrogenation properties of AlH_3 are closely related to kinetic inhibition effects. Thermodynamically it is unstable at room temperature [2,4,5,7]. Kinetic inhibition maintains the hydride in a metastable state under ambient conditions, but rapid dehydrogenation becomes possible at slightly elevated temperatures [1,6]. A more comprehensive understanding of these kinetic effects is crucial not only for enhanced control of the AlH_3 system but also for the development of thermally controlled hydrogen storage systems in general [1].

The origin of the kinetic inhibition effect is a matter of controversial debate [10–14]. To address this issue we have recently investigated [15] the role of native point defects in the dehydrogenation using density functional theory with the screened hybrid Hartree–Fock functional of Heyd, Scuseria, and Ernzerhof (HSE) [16,17]. We find that at thermodynamic dehydrogenation conditions positively charged hydrogen vacancies (V_H^+) are the dominant defects that mediate the mass transport in the bulk. The calculated activation energy for the self-diffusion of V_H^+ is in good agreement with experimental values for the activation energy of the dehydrogenation reaction of AlH_3, leading to the conclusion that the mass transport in the bulk, as mediated by the vacancies, is the kinetic bottleneck for the reaction.

In this paper we discuss in more detail the stability and mobility of defects other than hydrogen vacancies, such as interstitial atomic H_i and molecular hydrogen $H_{2,i}$. Furthermore, we carefully compare our results from the HSE calculations to corresponding results obtained with a conventional DFT generalized gradient approximation (GGA) functional, which is less computationally demanding, but also less accurate than the HSE approach.

2. Method

To study the formation and migration of point defects we focus here on the α-phase of AlH_3 (space group $R\bar{3}c$). The α-phase is the most stable at ambient conditions and up to high pressure (on the order of 10 GPa) [2,6,18].

To quantify the extent to which a defect X contributes to the dehydrogenation we calculate its activation energy for self-diffusion:

$$E_a[X] = E_b[X] + E^f[X] \quad (1)$$

Here, $E^f[X]$ is the formation energy of the defect and $E_b[X]$ is the energy barrier associated with migration of the defect within the crystal. As possible defects we have considered interstitial hydrogen in monatomic (H_i) and molecular ($H_{2,i}$) form,

* Corresponding author.
E-mail address: ismer@engineering.ucsb.edu (L. Ismer).

0925-8388/$ – see front matter © 2010 Elsevier B.V. All rights reserved.
doi:10.1016/j.jallcom.2010.10.014

Table 1
Lattice parameters of α-AlH_3.

	a (Å)	c (Å)
PBE	4.49	11.84
HSE	4.43	11.73
Ref. [23] (PBE)	4.49	11.82
Ref. [18] (exp.)	4.45	11.80

as well as hydrogen vacancies (V_H). Aluminum-related defects, i.e, interstitial Al and Al vacancies all have very high formation energies (> 2 eV). Therefore they do not play a significant role in dehydrogenation.

In our study we explicitly take into account that the point defects are in a charge state q. The formation energy of a hydrogen-related defect is defined as [19]:

$$E^f(X) = E_{tot}(X) - E_{tot}(AlH_3) + n\left(\frac{1}{2}E_{tot}(H_2) + \mu_H\right) + q\varepsilon_F, \quad (2)$$

where $E_{tot}(X)$ is the total energy of a supercell of the AlH_3 crystal containing one defect, and $E_{tot}(AlH_3)$ is the total energy of the perfect crystal in the same supercell. n is number of H atoms added to ($n<0$) or removed from ($n>0$) the supercell to form the defect. μ_H is the H chemical potential, referenced to the total energy of an isolated H_2 molecule $\left[\frac{1}{2}E_{tot}(H_2)\right]$, and ε_F is the electron chemical potential (Fermi level), referenced to the bulk valence-band maximum (VBM). The choices for ε_F and μ_H will be discussed below.

To determine the formation energies and the migration barriers of the defects we have performed first-principles calculations based on density functional theory (DFT) and periodic boundary conditions. All calculations were performed using the Vienna ab initio simulation package (VASP) [20]. The electronic wave functions are expanded in a plane-wave basis using the projector augmented wave approach. A cutoff of 300 eV was used to confine the size of the plane-wave basis. The defects were simulated using supercells containing 24 Al atoms and 72 H atoms; integrations over the Brillouin zone were performed by using a Γ-centered mesh of 2 × 2 × 2 k-points.

As mentioned above we have used and compared two different exchange-correlation (XC) functionals to perform our study: (1) a generalized gradient approximation (GGA) type XC functional, more specifically the PBE functional [21], and (2) the hybrid DFT/Hartree–Fock XC functional of Heyd, Scuseria, and Enzerhof [16,17]. For the exchange mixing parameter in HSE we used the default value of 0.25, i.e., one quarter of Hartree–Fock exchange and three quarters of PBE exchange.

To remove spurious contributions arising from interactions between defects and with the homogeneous compensation charge in charged supercell calculations we have applied the correction scheme of Ref. [22]. All equilibrium structures have been fully relaxed for the respective XC functional by using the quasi-Newton (QN) algorithm as implemented in VASP. The saddle points for defect migration have been determined by employing the climbing image nudged elastic band method.

3. Results

The lattice constants and band gap of AlH_3 according to the HSE and PBE calculations are listed in Table 1. For the lattice constants we find that both PBE and HSE agree well with experimental values [18]. For the validation of the accuracy of the band gap we compare here to a theoretical value obtained from a GW calculation [23] (E_g = 3.54 eV); no experimental value is available. PBE predicts a band gap of E_g = 2.12 eV, hence underestimates the band gap with respect to the GW value by 40%. This confirms the general trend reported in the literature for a broad range of materials: standard DFT-GGA underestimates the band gap of semiconductors and insulators by 30–50% (e.g., [24]). The HSE value for the band gap (E_g = 3.38 eV) is, as expected, in much better agreement with the GW value than the PBE value.

The formation energy of the defects depends on the hydrogen chemical potential μ_H and on the chemical potential for the electrons, i.e., the Fermi level ε_F [see. Eq. (2)]. In the present study we focus on dehydrogenation conditions when the material is exposed to air at normal conditions (T = 273 K, p = 1 atm). The H_2 content in air is approximately 5 ppm. According to the ideal gas approximation and considering the partial pressure of H_2 ($p_{H2} = 5 \times 10^{-6}$ atm), we arrive at a value of $\mu_H = -0.29$ eV. While our approach is different from the approach used in previous studies [25,26], we note that the actual value we chose for μ_H is close to the value used to describe H-poor conditions in the studies about MgH_2 [25] ($\mu_H = -0.33$ eV) and $NaAlH_4$ [26] ($\mu_H = -0.12$ eV).

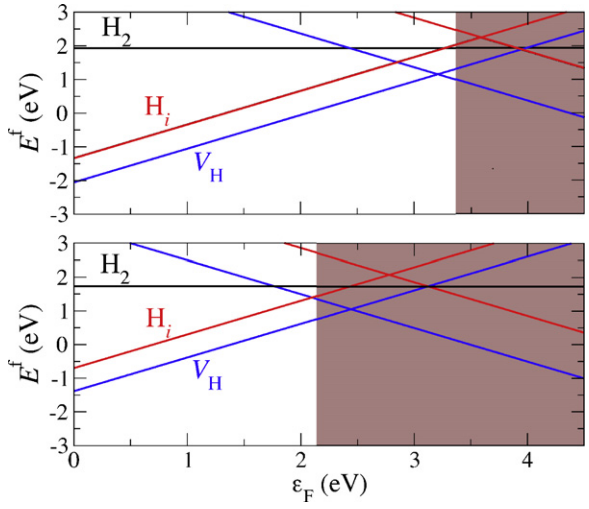

Fig. 1. Formation energies of hydrogen related point defects in α-AlH_3 calculated with HSE (upper plot) and PBE (lower plot): The formation energies are calculated for $\mu_H = -0.29$ eV (dehydrogenation conditions, see Eq. (2)). Negative slopes denote the negative, $q = -1$, charge state, positive slopes denote the positive, $q = 1$, charge state, and horizontal lines denote the neutral charge state. The white region of the plot denotes the band gap (starting from the valence-band maximum at $\varepsilon_F = 0$) and the shaded region denotes the conduction band.

To set a value for ε_F we observe that AlH_3 is a material in which the conduction-band minimum (CBM) occurs at a low energy on an absolute energy scale (with respect to the vacuum level), a result obtained from surface calculations as described below. It therefore has a strong intrinsic propensity for n-type behavior [27], and ε_F is expected to be near the CBM. We therefore set $\varepsilon_F = \varepsilon_{CBM}$. The resulting formation energies are shown in Fig. 1.

The formation energies, energy barriers and activation energies of the relevant defects for $\mu_H = -0.29$ eV and $\varepsilon_F = \varepsilon_{CBM}$ are listed in Table 2. The local geometries of the ground-state and transition-state structures obtained from the migration barriers of the individual defects are shown in Fig. 2. Regarding the migration of $H^0_{2,i}$, we have also considered the possibility that the molecule dissociates rather than stays in molecular form. Taking charge neutrality during the dissociation process into account, we find that the energy required for the dissociation of $H^0_{2,i}$ within the AlH_3 crystal exceeds 1.5 eV (unpublished work). Hence it is preferable for the molecule to remain bound during the migration process.

For both PBE and HSE we find that compared to the other defects (Table 2), the V^+_H defect has a low formation energy (i.e., high concentration) and a low migration barrier (i.e., high mobility). Overall, the positively charged vacancy (V^+_H) defect has the lowest activation energy. The H^0_2 and H_i defects have very high formation energies under dehydrogenation conditions, and hence are irrelevant for the decomposition reaction. The negatively charged hydrogen vacancy V^-_H has a relatively low formation energy, but a very high migra-

Table 2
Formation energies, migration barriers and activation energies for $\mu_H = -0.29$ eV and $\varepsilon_F = \varepsilon_{CBM}$.

Quantity	Functional	H^-_i	H^+_i	V^-_H	V^+_H	H^0_2
E^f (eV)	PBE	2.75	1.36	1.36	0.68	1.73
	HSE	2.45	2.08	0.97	1.34	1.91
E_b (eV)	PBE	0.16	0.62	1.15	0.32	0.86
	HSE	0.13	0.73	1.53	0.38	0.87
E_a (eV)	PBE	2.91	1.98	2.51	1.00	2.59
	HSE	2.58	2.81	2.50	1.72	2.78

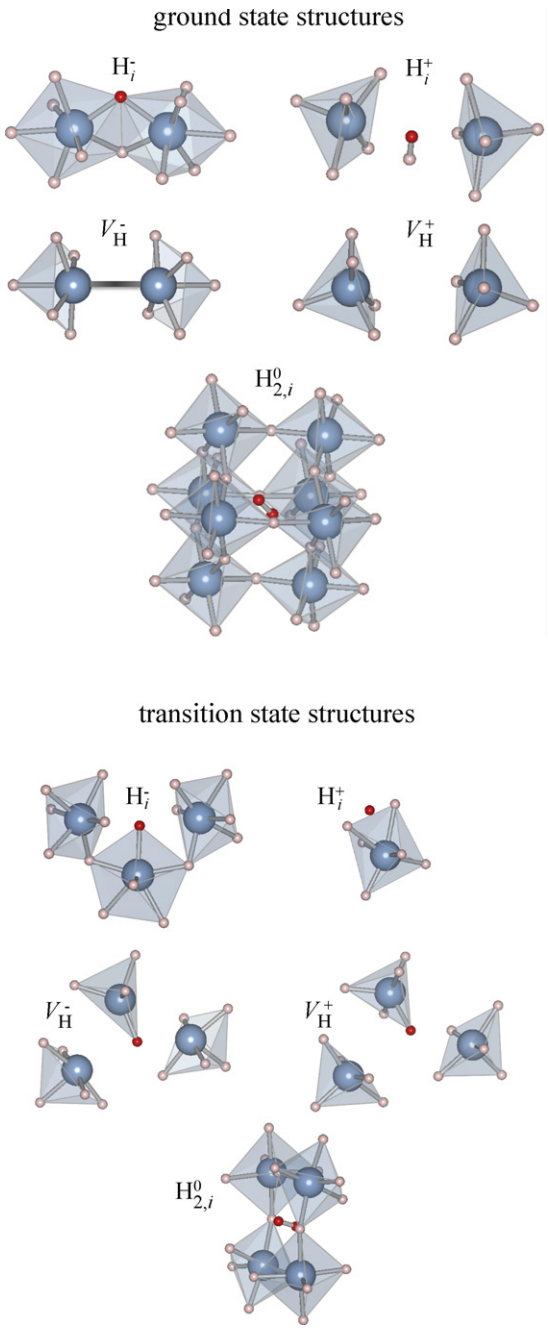

Fig. 2. Geometry of the ground-state and transition-state structures of the native point defects. The large blue balls denote Al atoms, whereas the small, white balls denote H atoms. The interstitial H atoms are colored red. The light bars denote Al–H bonds. The darker bar in the V_H^- ground-state structure denotes an Al–Al bond. (For interpretation of the references to colour in this figure legend, the reader is referred to the web version of the article.)

tion barrier. We can therefore conclude that the mass transport across the bulk during the dehydrogenation of AlH_3 is exclusively mediated by positively charged hydrogen vacancies (V_H^+) and that this mass transport is likely the rate-limiting mechanism of the dehydrogenation reaction [15].

While there is qualitative agreement between the PBE and the HSE results regarding the activity of the defects, large quantitative differences in the activation energies are observed (Table 2). For the V_H^+ defect HSE gives a value of E_a = 1.72 eV, which is good agreement with experimental values for the activation energy of the dehydrogenation reaction (1.62 ± 0.13, Ref. [28]). PBE, however, gives a

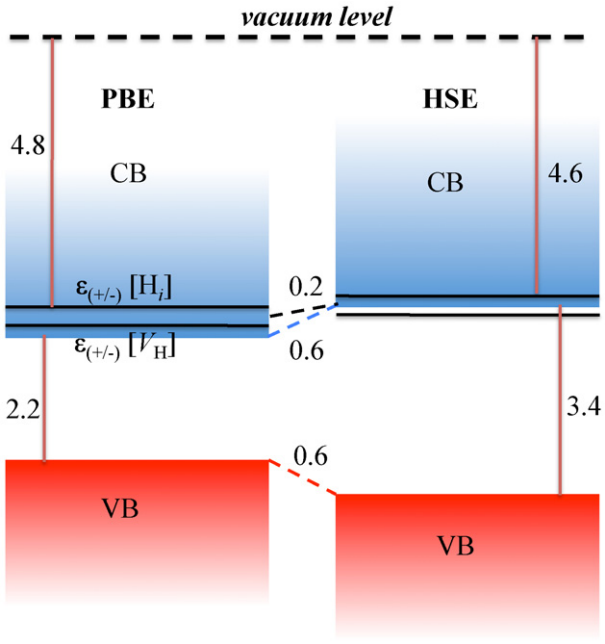

Fig. 3. Changes in the electronic eigenspectrum between the PBE and the HSE approach.

much lower activation energy of E_a = 1.0 eV, in clear disagreement with the experimental observations. We conclude that PBE severely underestimates the activation energy.

A closer inspection of our results reveals that the differences between PBE and HSE can be understood in terms of the different positioning of the $\varepsilon(\pm)$ charge-state transition levels relative to the band edges of the AlH_3 host. To examine these differences we need to align the HSE and the PBE band structures on an absolute energy scale. To determine the alignment we have performed surface calculations for AlH_3 with both PBE and HSE. The alignment shows that the band gap is widened for HSE compared to PBE by upshifting the CBM and downshifting the VBM, both by about 0.6 eV (Fig. 3). In contrast to the band edges, the transition levels do not substantially shift between the two functionals according to our calculation (Fig. 3), confirming a general trend reported in Ref. [29]; for H_i this confirms the universal alignment rule for the $\varepsilon(\pm)$ transition level claimed in Ref. [27].

Since the Fermi level is near the CBM, the stability of the charged defects changes approximately in the same way as the band edges shift between HSE and PBE, i.e., the formation energy of the positively charged defects is ~0.6 eV higher for HSE and the formation energy of the negatively charged defects is ~0.6 eV lower. We conclude that the strong differences in the activation energies are mainly an effect of the band-edge shifts. We note that the formation energy of the neutral H_2^0 defect differs by ~0.2 eV in HSE versus PBE. Some differences in migration barriers also occur (Table 2). However, for most defects these differences are smaller than the effect of the band-edge shift.

Finally, we note that the strong difference between PBE and HSE may be rather specific to AlH_3. In other hydrides, such as MgH_2 [30] and $NaAlH_4$ [31], the relevant point defects appear as pairs of oppositely charged defects (Frenkel pairs). In these systems, the differences between HSE and PBE will thus largely cancel out in the formation energies of the relevant defect complexes.

4. Conclusions

To summarize, we have identified the native point defects that contribute to dehydrogenation of α-AlH_3. The comparison

between DFT calculations with different functionals (PBE and HSE) reveals significant quantitative differences for the activation energies. Though PBE produces correct trends, an accurate prediction of absolute concentrations and activities of the defects requires a more advanced functional such as HSE.

Acknowledgements

This work was supported by the U. S. Department of Energy (Grant No. DE-FG02-07ER46434). It made use of the National Energy Research Scientific Computing Center, which is supported by the Office of Science of the U.S. Department of Energy under Contract No. DE-AC02-05CH11231 and the NSF-funded TeraGrid resources under Grant No. DMR07-0072N. L. I. thanks the UCSB-MPG Program for International Exchange in Materials Science and the NSF-IMI Program (DMR04-09848) for financial support.

References

[1] J. Graetz, Chem. Soc. Rev. 38 (2009) 73.
[2] J. Graetz, S. Chaudhuri, Y. Lee, T. Vogt, J.T. Muckerman, J.J. Reilly, Phys. Rev. B 74 (2006) 214114.
[3] P. Vajeeston, P. Ravindran, H. Fjellvag, Chem. Mater. 20 (2008) 5997.
[4] S. Sun, X. Ke, C. Chen, I. Tanaka, Phys. Rev. B 79 (2009) 024104.
[5] J. Graetz, J.J. Reilly, J. Alloys Compd. 424 (2006) 262.
[6] H. Saitoh, A. Machida, Y. Katayama, K. Aoki, Appl. Phys. Lett. 93 (2008) 151918.
[7] C. Wolverton, A. Ozolins, M. Asta, Phys. Rev. B 69 (2004) 144109.
[8] L. Ismer, M.S. Park, A. Janotti, C.G. Van de Walle, Phys. Rev. B 80 (2009) 184110.
[9] R. Zidan, B.L. Garcia-Diaz, C.S. Fewox, A.C. Stowe, J.R. Gray, A.G. Harter, Chem. Commun. (2009) 3717.
[10] J. Graetz, J.J. Reilly, J. Phys. Chem. B 109 (2005) 22181.
[11] G. Sandrock, J. Reilly, J. Graetz, W.-M. Zhou, J. Johnson, J. Wegrzyn, J. Alloys Compd. 421 (2006) 185.
[12] S.D. Beattie, T. Humphries, L. Weaver, G.S. McGrady, Chem. Commun. (2008) 4448.
[13] L. Senadheera, E.M. Carl, T.M. Ivancic, M.S. Conradi, R.C. Bowman Jr., S.-J. Hwang, T.J. Udovic, J. Alloys Compd. 463 (2008) 1.
[14] S. Kato, M. Bielmann, I. Kazutaka, S. Orimo, A. Borgschulte, A. Züttel, Appl. Phys. Lett. 96 (2010) 051912.
[15] L. Ismer, A. Janotti, C. Van de Walle, 2010, unpublished.
[16] J. Heyd, G.E. Scuseria, M. Ernzerhof, J. Chem. Phys. 118 (2003) 8207.
[17] J. Heyd, G.E. Scuseria, M. Ernzerhof, J. Chem. Phys. 124 (2006) 219906.
[18] J.W. Turley, H.W. Rinn, Inorg. Chem. 8 (1969) 18.
[19] A. Peles, C.G. Van de Walle, Phys. Rev. B 76 (2007) 214101.
[20] G. Kresse, J. Furthmüller, Phys. Rev. B 54 (1996) 11169.
[21] J.P. Perdew, K. Burke, M. Ernzerhoff, Phys. Rev. Lett. 77 (1996) 3865.
[22] C. Freysoldt, J. Neugebauer, C.G. Van de Walle, Phys. Rev. Lett. 102 (2009) 016402.
[23] M.J. van Setten, V.A. Popa, G.A. de Wijs, G. Brocks, Phys. Rev. B 75 (2007) 035204.
[24] M.C. Payne, M.P. Teter, D.C. Allan, T.A. Arias, J.D. Joannopoulos, Rev. Mod. Phys. 64 (1992) 1045.
[25] M.S. Park, A. Janotti, C.G. Van de Walle, Phys. Rev. B 80 (2009) 064102.
[26] G.B. Wilson-Short, A. Janotti, C.G. Van de Walle, Phys. Rev. B 80 (2009) 224102.
[27] C.G. Van de Walle, J. Neugebauer, Nature 423 (2003) 626.
[28] P.J. Herley, O. Christofferson, J. Phys. Chem. 85 (1981) 1887.
[29] A. Alkauskas, P. Broqvist, A. Paquarello, Phys. Rev. Lett. 101 (2008) 046405.
[30] M.S. Park, A. Janotti, C.G. Van de Walle, Phys. Rev. B. 80 (2009) 064102.
[31] G.B. Wilson-Short, A. Janotti, K. Hoang, A. Peles, C.G. Van de Walle, Phys. Rev. B 80 (2009) 224102.